

Novel Bilirubin Quantification Method: Computational and *In Vitro* Validation

By:

William Adu-Jamfi, Gabriella Haiz, Kaitlyn Hixson, Mark Provost

University of Virginia, Department of Biomedical Engineering Spring 2024

Faculty Advisors:

William Guilford, Department of Biomedical Engineering

Brian Helmke, Department of Biomedical Engineering

Word Count: 6489



Number of Figures: 8

Number of Tables: 0

Number of Equations: 14

Number of Supplements: 6

Number of References: 23

Approved:  Date: 5/6/2024


Novel Bilirubin Quantification Method: Computational and *In Vitro* Validation

William Adu-Jamfi^a, Kaitlyn Hixson^a, Gabriella Haiz^a, Mark Provost^a, Brian Helmke^{b,1}, William Guilford^{b,1}

^a UVA Department of Biomedical Engineering, Undergraduate

^b UVA Department of Biomedical Engineering

¹ Correspondence: William Guilford and Brian Helmke, Department of Biomedical Engineering

Abstract

Neonatal jaundice presents a common challenge in newborn care due to elevated bilirubin levels. Phototherapy, a standard treatment, uses blue light to photoconvert bilirubin into a more water-soluble isomer, lumirubin, facilitating its excretion. However, existing transcutaneous bilirubinometers often overestimate bilirubin levels in infants with darker skin tones, potentially leading to unnecessary phototherapy treatments and adverse side effects that create racial healthcare disparities. To address this, a novel non-invasive method utilizing bilirubin photoconversion has been proposed and tested by the previous Capstone team. This method measures bilirubin concentrations by assessing the exponential decay of absorbance during blue light exposure. A comprehensive study integrating experimental and computational approaches was conducted to validate this method's efficacy in a more complex and physiologically relevant system.

Experimental models, including *in vitro* flow dialysis and computational partial differential equation (PDE) models, were employed to mimic bilirubin diffusion and photoconversion. The *in vitro* model confirmed diffusion and photoconversion mechanisms, while the analytical PDE model successfully exhibited diffusion out of the control volume and accurately approximated experimental outcomes. This coupled approach aids the understanding of bilirubin transport from hydrophobic to hydrophilic environments within the body.

Results showed moderate to good correlation between experimental and theoretical data, with diffusion-reaction experiments exhibiting the highest predictive capacity. Challenges and limitations included the physiological accuracy of the experimental setup and literature gaps in the characterization of bilirubin and lumirubin transport *in vivo*. Future directions include implementing a system of PDE equations that integrates bilirubin and lumirubin, incorporating additional factors such as albumin and skin chromophores into the *in vitro* experiments for enhanced physiological representation, and additional validation of the predictive capacity of the analytical model. Overall, this research offers a promising approach for non-invasive bilirubin measurement, potentially mitigating racial biases in neonatal jaundice diagnosis and treatment.

Keywords: bilirubin, melanin, absorbance, photoisomerization, phototherapy, bilirubinometer

Introduction

Neonatal jaundice, also known as hyperbilirubinemia, is a common condition characterized by a yellowish hue in the skin of many newborns. It is caused by a build-up of bilirubin in the blood and occurs through two simultaneous occurrences. First, there is an increase in bilirubin production due to the higher breakdown of fetal red blood cells, which is caused by the shorter lifespan of these cells and the larger amount of red blood cells in newborns. Secondly, there is a low capacity for hepatic excretion due to low levels of the binding protein ligandin in hepatocytes and reduced activity of glucuronyl transferase, the enzyme that conjugates bilirubin to glucuronic acid, allowing it to become water-soluble. Therefore, unconjugated bilirubin accumulates in the neonate's blood, leading to elevated levels of total serum bilirubin (TSB). While the mother's liver eliminates bilirubin for the baby during pregnancy, after birth, the baby's liver must do this job. However, in some infants, the liver may not yet be sufficiently mature to effectively eliminate bilirubin, allowing an excessive amount of unconjugated bilirubin to build up in a newborn's bloodstream.¹

Roughly 50% of full-term and 80% of premature infants experience jaundice within their first week of life.² Vigilant and precise monitoring of bilirubin levels is crucial, as untreated or undetected hyperbilirubinemia can result in serious complications such as encephalopathy, hearing impairment, and kernicterus—a lifelong neurological disorder characterized by various symptoms including cerebral palsy, impaired upward gaze, dental enamel abnormalities, hearing loss, and developmental coordination issues.³

Phototherapy

To prevent the complications of hyperbilirubinemia, approximately 10% of full-term and 25% of premature newborns may require phototherapy, which involves the strategic use of blue light to decrease TSB.⁴ The photoconversion of bilirubin in the skin (TcB) into lumirubin, a more water-soluble and easily excreted photoisomer, facilitates its removal through the bile and urine. Unlike bilirubin, which tends to be stored in fatty tissues, lumirubin is

more soluble in the body's aqueous solutions, making it easier for the body to eliminate without relying heavily on the liver, which is not fully developed in newborns and is a major factor in hyperbilirubinemia.⁵

Existing Measurement Methods

Neonatal jaundice monitoring and diagnosis currently depends on two approaches. The gold standard involves directly measuring TSB by taking venous or heel stick blood samples. Although accurate, this procedure is painful, invasive, and carries significant health risks, including a higher likelihood of hospital-acquired infections, particularly in newborns.⁶ Additionally, heel pricks pose risks such as accidentally puncturing the heel bone or causing joint issues, which could lead to cartilage and bone damage. Furthermore, to continually monitor TSB levels and observe fluctuations, healthcare professionals often need to repeatedly prick newborns in the same spot, further complicating the healing process in a patient group already susceptible to infections due to their underdeveloped immune systems.⁷

As an alternative approach to minimize these health risks, transcutaneous bilirubin screening measures TcB levels non-invasively. Non-invasive transcutaneous bilirubinometry employs a handheld bilirubinometer, which emits specific light wavelengths into the skin and analyzes the reflected light's spectrum. The variations in this spectrum are dependent on the wavelengths of light absorbed by various skin components, including bilirubin, hemoglobin, and melanin, and the degree of light absorption by the skin serves as an indicator of bilirubin concentration.⁸ These non-invasive measurements offer a quantitative assessment of the risk for infants who may develop severe jaundice or bilirubin encephalopathy, facilitating timely clinical decisions, especially in regions with limited access to traditional laboratory tests.⁹

The Limitations of Current Transcutaneous Bilirubinometers

Currently, non-invasive transcutaneous bilirubinometers often overestimate bilirubin levels in neonates with darker skin tones, characterized by higher cutaneous melanin

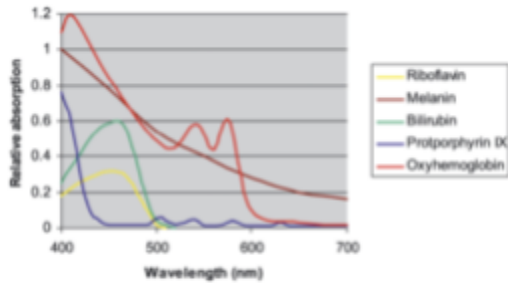


Figure 1: Comparative absorption profiles of typical skin pigments in the spectral range of 400 to 700 nm¹¹

concentrations, reducing the effectiveness of TcB screening in this racial group.¹⁰ This issue arises from a significant overlap in the absorption spectra of bilirubin and melanin, as illustrated in *Figure 1*. Notably, melanin's absorption is particularly prominent near the peak absorbance of bilirubin, which is the optimal wavelength for detecting or monitoring bilirubin concentration. Moreover, melanin's absorption is consistently higher than bilirubin at various points across the spectra. Consequently, higher cutaneous melanin levels can effectively obscure variations in bilirubin absorption, making it more difficult to accurately assess bilirubin concentrations in the skin.^{11,12} This overlap commonly leads to an overestimation of TcB, as most bilirubinometers misinterpret the increased absorption as indicative of higher bilirubin levels.⁸

The overestimation of bilirubin levels poses several risks, primarily increasing the chances of neonates receiving phototherapeutic treatment for jaundice. Although this therapy has historically been deemed safe, recent research has brought to light potential side effects that were previously not fully understood. These adverse effects encompass short-term consequences, including disturbances in the neonatal thermal environment, water loss, electrolyte imbalances, disruptions in liver function, alterations in the newborn's circadian rhythm, and interference with early-stage maternal-infant interactions. Moreover, specific studies have hinted at the possibility of long-term consequences, such as the development of melanocytic nevi, skin cancer, allergic diseases, and retinal damage.¹³ Given the issue of TcB overestimation in neonates with darker skin tones,

their heightened likelihood of receiving phototherapeutic treatment points to an unintentional introduction of racial bias into bilirubinometers. The racial bias inherent in the current approach for obtaining accurate transcutaneous bilirubin readings disproportionately affects these individuals, restricts their access to equitable healthcare, and contributes to larger issues of racial health disparities on a global scale

Overview of Solution and Prior Work

A novel method for a non-invasive and skin-tone inclusive bilirubin quantification method has been proposed by a prior capstone group that takes advantage of the photoconversion capacity of bilirubin. Bilirubin photoconverts into the photoisomer lumirubin under blue light, which has a different absorbance spectrum. By continuously illuminating one location with blue light, the photoconversion of bilirubin can be measured with optical absorbance measurements at 460 nm, the peak absorbance wavelength of bilirubin. As the absorbance of bilirubin decreases exponentially, due to the photoconversion and movement of lumirubin out of the tissue, the steady state of the concentration decrease, shown as the asymptote of absorbance at 460 nm over time, can be used to calculate the initial concentration of bilirubin in the skin as shown in *Figure S1* and *Figure S2*.

The previous capstone group demonstrated a proof-of-concept for the use of photoconversion to estimate initial bilirubin concentration in a simplified system. First, they sought to better understand the photoisomerization of bilirubin. To relate absorbance to concentration, they photobleached three different bilirubin-only solutions at varying concentrations. Absorbance was measured at regular intervals over 200 minutes, and an exponential decay curve was fitted to the absorbance measurements at 460 nm for each solution. The exponential decay took the form of Equation S1. They defined the initial amount coefficient of the fitted equation as the alpha value (α), which represents the change in absorbance if the solution is photobleached infinitely, with the assumption that after an infinite time all bilirubin would be photoconverted and would have minimal absorbance at 460 nm. They defined the delta value as the difference between

the initial ($Abs_{t=0}$) and final ($Abs_{t=end}$) absorbance measurements, shown in Equation S2. Linear standard curves for the alpha values and delta values of the different bilirubin-only solutions were created to quantify the relationship between change in absorbance and initial concentration. The linear standard curves for the alpha and delta values each had an $r^2=0.997$, indicating a good fit.

To determine the effect of melanin on the use of photoconversion to measure initial bilirubin concentration, solutions of high melanin/high bilirubin, high melanin/low bilirubin, low melanin/high bilirubin, and low melanin/low bilirubin were made. The high and low concentrations for both melanin and bilirubin were informed by the physiological range for each compound. All of the solutions were continuously exposed to blue light and allowed to photoisomerize over the span of 200 minutes and absorbance at 460 nm was measured periodically to capture the exponential decay of absorbance as the solutions were photobleached, shown in *Figure S1* and *Figure S2*. Using the alpha and delta linear standard curves, initial concentrations were predicted for each condition and error was calculated between the predicted and measured initial concentrations. The overall average percent error of both the alpha and delta value predictions of concentration was $9.44\% \pm 10.3\%$, with no difference in accuracy for the high melanin solutions. Overall, this work indicates that using the decreasing absorbance values at 460 nm from a continuously photoisomerized site can predict initial bilirubin concentrations with reasonable accuracy, regardless of melanin concentration.¹⁴

While this work demonstrates proof-of-concept for this method, it was performed in cuvettes, with only bilirubin photoconversion causing the decrease in absorbance at 460 nm. This system is highly simplified and does not seek to represent other physiological mechanisms of bilirubin movement, such as diffusion from blood to skin. This work also used a basic buffer as the solution in which bilirubin and melanin were dissolved, which is not representative of the hydrophobic environment within the skin where bilirubin accumulates in jaundice. Additionally, while they also created an analytical Ordinary Differential Equation (ODE) model showing the relative

change in concentration of bilirubin photoisomers during photoconversion over time, it only represented the chemical reaction that leads to bilirubin concentration decrease and it did not include a spatial component. This capstone project seeks to provide further validation of the method of using absorbance values during photoconversion to determine initial bilirubin concentration in a more complex and physiologically relevant system. This coupled computational and *in vitro* experimental system accounts for both diffusion and reaction within a hydrophobic control volume that simulates multiple mechanisms of bilirubin movement within the skin.

Results

In Vitro Flow Dialysis Model

First, a calibration curve for bilirubin in octanol was created to relate absorbance measurements to concentrations (see *Figure S3*). The linear range obtained from the calibration curve was approximately .001 to .01 mg/mL, and the estimated detection limit was 0.0004 mg/mL, which was estimated from the x-intercept. For the diffusion-only experiments ($n = 3$), a slight decrease in absorbance over time was seen as compared to the experiments containing photoconversion reactions with blue light. For the reaction-only ($n = 3$) and diffusion-reaction ($n = 3$) experiments, an exponential decay curve was fitted based on the computational model. A plot of the diffusion-only, reaction-only, and diffusion-reaction curves with mean and error bars can be seen in *Figure 2*.

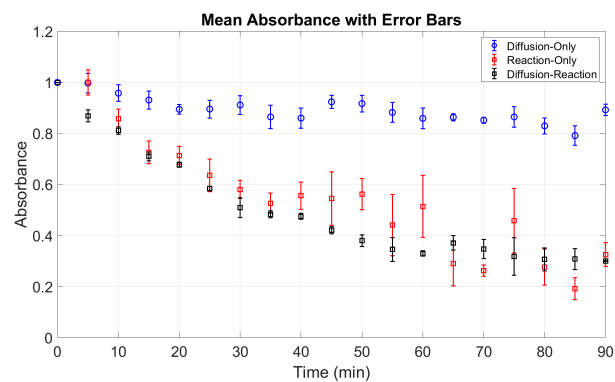


Figure 2: Mean absorbance with error bars for diffusion-only, reaction-only, and diffusion-reaction experiments ($n = 3$ for each

experimental condition). The error bars represent the standard error of the mean.

Computational Model

First, the behavior in concentration produced by the pdepe solution matches with the numerically approximated solution of Equation 1 calculated using the pdepe solver in MATLAB. The results from the MATLAB pdepe solver are shown in Figure 3.

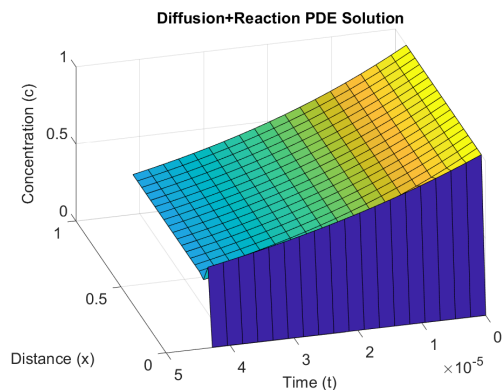


Figure 3: MATLAB pdepe solution matches with analytical solution of diffusion-reaction equation

Both temporal and spatial slices demonstrate an overall decrease in bilirubin concentration, shown in Figure S4. This indicates that bilirubin concentration is non-uniformly dispersed into adipose tissue as a result of diffusion and photoconversion.

To investigate the predictive power of the PDE model, the theoretical data was compared to the experimentally collected data. Initially, to test the accuracy of the theoretical equations in demonstrating bilirubin behavior *in vitro*, the experimental data was compared to Equation 3 & 5 for diffusion-only, reaction-only, and diffusion-reaction experiments.

For each experimental condition, the average of the three trials were plotted against the theoretically calculated data points. The majority of the experimental data points for the diffusion-only condition did not fall within the 95% confidence interval of the regression model, as shown in Figure 4. The r^2 value for the experimental data and the model was found to be 0.03. An ANOVA test was completed using an F statistic to compare the experimental data and

theoretical values and returned a p-value of 0.18, meaning that the exponential, or theoretical, fit does not describe the data well. This proved to be not significant at the 95% level. The diffusion-only model exhibited the least amount of predictive capacity out of the three experimental models.

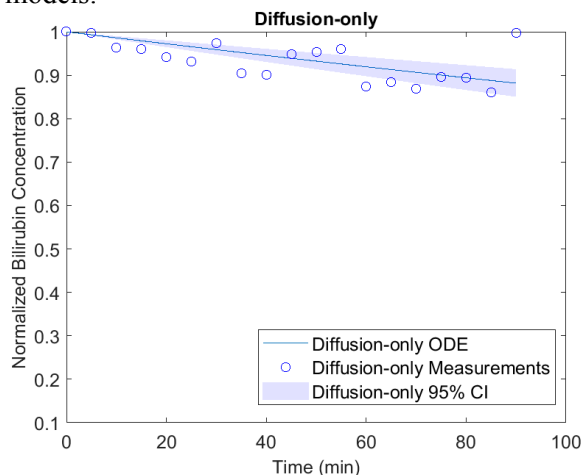


Figure 4: Diffusion-only experimental data compared to a theoretically calculated curve with 95% confidence intervals

For the reaction-only experiments, more data points were observed to fall in the 95% confidence interval, as shown by Figure 5. The r^2 value for the experimental data and the model was found to be 0.6. This indicates that there is a moderate correlation between the data and the model. An ANOVA test was completed and returned a p-value of 2.085×10^{-12} , indicating that there was a good fit between the model and the data for the reaction-only experiments. This proved to be significant at the 95% level.

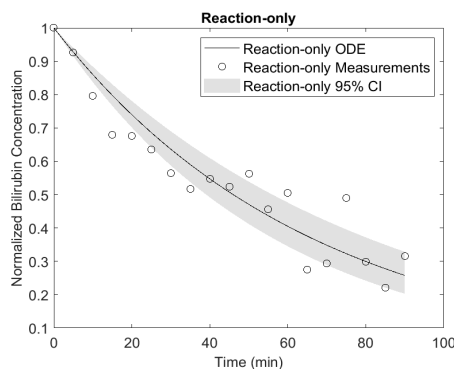


Figure 5: Reaction-only experimental data compared to a theoretically calculated curve with 95% confidence intervals

Notably, there are a similar amount of data points that fall within the 95% confidence interval for the diffusion-reaction experimental data compared to the other experimental conditions, as shown in *Figure 6*. The r^2 value for the experimental data and the model was found to be 0.73, exhibiting moderate correlation. An ANOVA test was completed and returned a p-value of 2.92×10^{-17} , indicating that the exponential fit captured the data especially well. This proved to be significant at the 95% level.

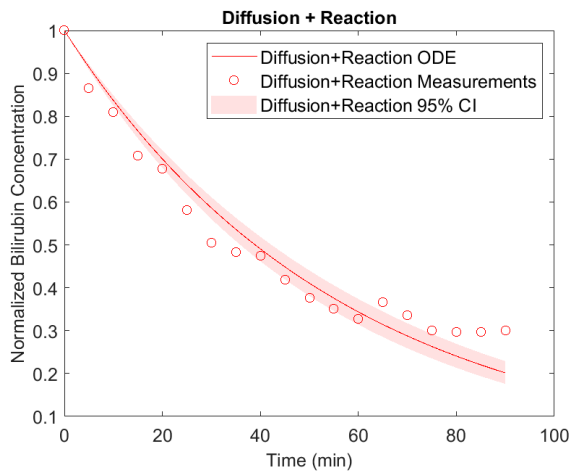


Figure 6: Diffusion-reaction experimental data compared to theoretically calculated with 95% confidence intervals

Finally, the experimental data was compared to the solution generated by the MATLAB pdepe solver.²⁰ This solution was derived from Equation 2. As shown in *Figure 7*, the experimental data was plotted against the PDE calculated solution, with one standard deviation error bars at each experimental point. It is important to note that the experimental points were averaged across the three trials related to diffusion-reaction. An ANOVA test was performed and returned a p-value of 2.29×10^{-13} . This indicates that there was a good fit between the experimental data and the model, and that there is some degree of predictive capacity. This proved to be significant at the 95% level.

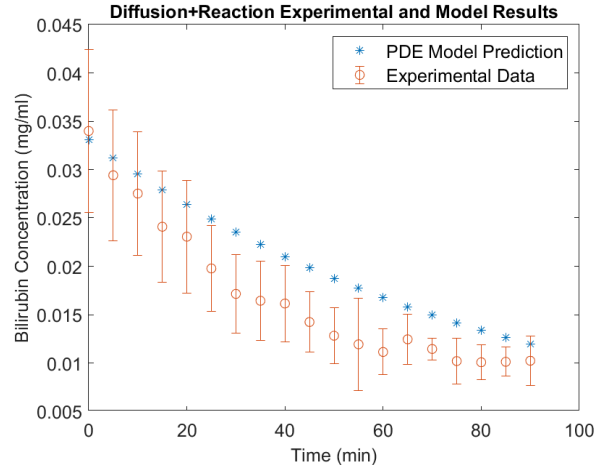


Figure 7: Analytical PDE model successfully integrates diffusion and reaction within one standard deviation to recreate in vitro conditions

Discussion

Significance & Innovation

To allow for noninvasive, skin tone inclusive, bilirubin measurement, alternate approaches with varying applications have been developed. Novel mobile applications, including Bilicam and neoSCB, have been created to allow for bilirubin screening. Bilicam uses images of the sternum as well as a calibration card to estimate TSB using machine learning. NeoSCB uses images of the sclera of the eye taken with and without flash to measure sclera chromaticity, and pilot studies have shown a good correlation with TSB values.¹⁵ Although these applications have shown preliminary success, they are primarily designed to be used as a screening tool outside of the clinical setting. Other skin tone inclusive solutions to measuring bilirubin concentration include an assay that also takes advantage of the photoconversion ability of bilirubin, but in reverse. This solution uses reverse blue light photoconversion of lumirubin excreted in urine into bilirubin along with the fluorescent protein UnaG.¹⁶ However, this method is primarily designed to be used as an assay, not a point of care device. In contrast to these alternative noninvasive, skin tone inclusive bilirubin measurements, the innovative method described above can be further developed to be

integrated into a device that can be used in clinical settings to monitor bilirubin concentration more continuously.

The *in vitro* model, designed to replicate bilirubin transport in the body, showcased consistency with the mass-transport ODEs, effectively demonstrating both diffusion and photoconversion. Additionally, the analytical PDE model successfully portrayed diffusion out of the control volume, aligning well with the expected solution. The analytical PDE model also successfully approximated experimental data, with the predicted data falling within one standard deviation of the experimental data. This illustrates that the model can successfully predict diffusion and photoconversion concentration profiles of bilirubin, which aids in the understanding of its movement from hydrophobic environments such as octanol or fat to hydrophilic environments such as water or blood. These models not only advance our comprehension of bilirubin transport in a well-characterized system but also hold promise for informing clinical strategies aimed at mitigating neonatal jaundice-related complications.

Challenges and Limitations

One challenge encountered was the literature gap in the quantification of the mechanisms of bilirubin and lumirubin movement between the bloodstream and the fat within the skin. The relative rates of the diffusion of bilirubin into the skin and the photoconversion reaction to remove bilirubin *in vivo* are not well characterized. Determining the relative rates of bilirubin entering and leaving the control volume is critical to the success of using bilirubin photoconversion to determine initial concentration, because if bilirubin is accumulating in the control volume faster than it is being photoconverted, this method will not accurately measure initial concentration because

an asymptote of absorbance at 460 nm will not be reached. To overcome this challenge, a more physiologically accurate *in vitro* model is needed to quantify bilirubin and lumirubin movement.

One limitation of the *in vitro* model is the use of octanol to simulate fat in the skin and water to simulate blood flow. Although octanol is hydrophobic and has a well characterized partition coefficient with water, there are structural differences between the use of a hydrophobic liquid and the inhomogeneous layer of adipocytes and extracellular matrix components of subcutaneous layers. Similarly, water is an extremely simplified analog of whole blood. In addition to erythrocytes and white blood cells, there are circulating proteins and other molecules in blood that could impact the diffusion of bilirubin out of the blood that are not represented by water. An important protein for bilirubin transport, albumin, was also not included, so the physical model only accounted for unconjugated bilirubin movement.

One limitation of the computational model is the reliance on the diffusion-reaction *in vitro* model that is not completely physiologically representative for the diffusivity and reaction rate parameters *in vivo*. This means that the model results are specific to the *in vitro* experimental setup described in the methods and are not more broadly representative of bilirubin movement *in vivo*. Additionally, for diffusion-only experiments, *in vitro* experiments had large experimental variability and did not have a statistically good fit with what the diffusion-only ODE would predict, which has implications for the value of free diffusivity used in the analytical model. This value was derived from the assumption that the diffusion-only ODE solution would adequately describe the experimental data, allowing the parameters of that fit to be used to calculate free diffusivity. However, since the diffusion-only ODE was not

a statistically good fit with the experimental data, other estimates of diffusivity may be needed.

Future Work

To make the system more physiologically relevant, it would be useful to implement a system of PDE equations related to bilirubin and the photoisomer, lumirubin. This would allow for a more accurate representation of the mechanisms that occur during phototherapy. Both PDE equations would consider the same spatial and temporal components that the current bilirubin PDE equations account for. This would provide insight on the relationship between bilirubin and lumirubin in the measurement of bilirubin concentration. A layer of complexity would also be added to the model that represents the true nature of bilirubin transport processes due to photoconversion.

More validation of the predictive capacity of the analytical model would further solidify the potential for implementation in a non-invasive bilirubin measurement device. The current system that has been developed is fairly simple and would require a higher degree of complexity before use in the clinical setting. Simultaneously, there should be more robust testing and validation of the model to ensure a higher degree of accuracy.

For the *in vitro* model, the next immediate step would be incorporating bilirubin and albumin into the dialysate. Given the hydrophobic nature of unconjugated bilirubin, its transport in plasma relies heavily on albumin binding. By introducing a continuous flow of bilirubin and albumin into the dialysate, we can achieve greater complexity and physiological accuracy in our experiments. Moreover, to further validate the inclusivity of this method, the integration of skin chromophores such as melanin and oxyhemoglobin into the *in vitro* experiments would be crucial. This would not only enhance the model's representation of diverse skin

tones but also bolster its relevance in clinical contexts.

Materials and Methods

In Vitro Physical Model

To create the calibration curve for bilirubin, a concentration of bilirubin in octanol of 0.01 mg/mL was created and serial dilutions were created to form the range of concentrations used to create the curve seen in *Figure S3*. A concentration of 0.01 mg/mL was chosen because this was calculated to be the maximum solubility of bilirubin in octanol. This was calculated with an estimate of the solubility of bilirubin in water of 100 nM.¹⁷ Using an estimated logP partition coefficient of 3.22 for bilirubin from an online tool provided by the Virtual Computational Chemistry Laboratory¹⁸, the solubility in octanol was calculated to be 0.01 mg/mL. Absorbance measurements for the calibration curve and all experiments were collected using a NanoDrop One. A standard volume of 2 μ L was taken for all samples run in the NanoDrop. Values of absorbance at the peak of 460 nm were used.

In order to make concentrations of bilirubin in octanol for the experiments, 1 mg of bilirubin was added to a tube containing 2 mL of octanol and 2 mL of water. The mixture was shaken well and allowed to settle for a few minutes so undissolved bilirubin would fall from the octanol. 1 mL of octanol was removed from the tube and transferred to a 1.5 mL microcentrifuge tube. The octanol with bilirubin was centrifuged at 14,000 rpm for 4 minutes to collect undissolved bilirubin at the bottom of the microcentrifuge tube. The solution used for experiments was then taken from the octanol with care not to take any undissolved bilirubin at the bottom of the microcentrifuge tube.

For the reaction-only experiments, 1 mL of dissolved bilirubin in octanol was added to a disposable cuvette. Blue light was shone on the cuvette at a distance of 85 mm and 3 measurements were taken every 5 minutes for 90 minutes. The 3 samples were averaged per time point to account for potential errors in pipetting, which was done for the diffusion-only and diffusion-reaction experiments as well.

In order to model the transport of bilirubin between blood and skin, a flow dialysis unit was used which can be seen in *Figure S5*. The unit consists of 3 plastic pieces: a bottom piece with two posts meant to guide the fit of the other two pieces, a middle piece that creates an oval shaped chamber with the bottom piece and has attachments for inflow and outflow of water and five holes on its top, and a top piece that contains five holes that create five wells. The dialysis membrane is placed between the middle and top pieces and o-rings are placed around each of the five holes to create a seal. The whole unit is clamped externally to make it watertight.

For diffusion-only experiments, 400 μL of bilirubin dissolved in octanol was added into one of the wells and 3 samples were taken every 5 minutes for 90 minutes. 400 μL was chosen as the sample volume because the wells have a maximum volume of 500 μL .

For diffusion-reaction experiments, the experimental setup using the flow dialysis unit can be seen in *Figure 8*.

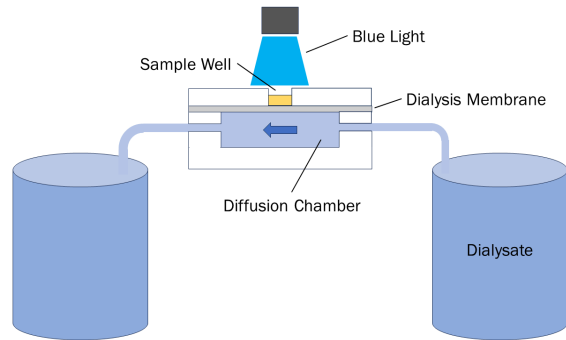


Figure 8: Diagram of the flow dialysis experimental setup for diffusion-reaction experiments.

Bilirubin dissolved in octanol filled the sample well and DI water was used for the dialysate. Octanol was chosen as the solution to represent the fat in the skin because it is hydrophobic and is used as a component in the n-octanol-water partition coefficient. By using octanol and water in the experiment, the transport of bilirubin can be better understood using our understanding of partition coefficients. The water was pumped through the flow dialysis unit using a peristaltic

pump. The sample well and diffusion chamber were separated by a dialysis membrane with a molecular weight cutoff of 10,000 Da. The blue light was held stationary at 85mm directly above the sample well using a custom 3D printed fixture. For experiments with blue light, only well 3 was used to ensure consistent and direct application of the blue light. The flow dialysis unit was placed on a magnetic stirrer which spun a stir bar at 1000 rpm inside the diffusion chamber to ensure the water in the chamber was well mixed.

Analytical PDE Model

Using conservation of mass, a Partial Differential Equation (PDE) that includes both diffusion and chemical reaction terms was created, shown in Equation 1. Steady state was not assumed. The control volume was established as a well in the flow dialysis chamber and did not include the dialysis membrane, which is why free diffusivity, D_{ij} , is used in the diffusion term of the PDE. The equation was only applied to one spatial dimension, the length of the well, L . The reaction term, R , was assumed to be first order, as represented by Nii et al., with the change in concentration being a product of the reaction rate, k , and the concentration of bilirubin.¹⁹

$$\frac{\partial C}{\partial t} = D_{ij} \frac{\partial^2 C}{\partial x^2} + R \quad [\text{Eq. 1}]$$

To make the model easily scalable, Equation 1 was converted into a dimensionless form, shown in Equation 2. The dimensional concentration was divided by the initial concentration (C_0), shown in Equation 2.1. The dimensional distance was divided by the length of the well, shown in Equation 2.2. The Fourier number was used to define dimensionless time, shown in Equation 2.3. Dimensionless definitions were substituted into Equation 1 to derive Equation 2.

$$\frac{\partial C^*}{\partial t^*} = \frac{\partial^2 C^*}{\partial x^{*2}} - k \left(\frac{L^2}{D_{ij}} \right) C^* \quad [\text{Eq. 2}]$$

$$C^* = \frac{C}{C_0} \quad [\text{Eq. 2.1}]$$

$$x^* = \frac{x}{L} \quad [\text{Eq. 2.2}]$$

$$t^* = \frac{tD_{ij}}{L^2} \quad [\text{Eq. 2.3}]$$

The solution to Equation 2 was solved and visualized using the PDE solver pdepe in MATLAB.²⁰ The initial condition was C_0 , which was equal to one in the dimensionless model. The boundary conditions were defined to be concentration equal to zero at the bottom boundary of the well and flux equal to zero at the top of the well. The left boundary condition was based on the assumption that there was no amount of bilirubin outside of the well. The right boundary condition assumed that the concentration of bilirubin at the membrane was essentially zero due to the large dilution when it entered the water-only dialysate and the convection that removed the bilirubin after it crossed the membrane.

The free diffusivity and reaction rate parameters were obtained from fitting mass balance ODEs for diffusion-only and reaction-only to diffusion-only flow dialysis experiments and reaction-only experiments. The solution of the mass balance ODE for diffusion-only is shown in Equation 3. This equation was fit to the experimental data to solve for $\frac{-k_p}{l}$, with k_p representing a mass transport coefficient that accounts for the hindrance of the membrane and l representing the thickness of the membrane. The hydrated membrane thickness was measured to be 85 μm .

$$C(t) = C_0 e^{-\frac{k_p}{l}t} \quad [\text{Eq. 3}]$$

The free diffusivity was related to k_p by Equation 4. In this equation T is the tortuosity of the membrane, which was assumed to be 1.1. ϵ is the porosity of the membrane, which was assumed to be 0.8 based on literature measurements of a dialysis membrane with a similar composition.²¹ β is the partition coefficient, which is calculated in Equation S3 in the appendix using λ , which is the ratio of the solute diameter and the membrane pore diameter, shown in Equation S4 in the appendix. The solute diameter was estimated with an empirical estimation, shown in Equation

S5 in the appendix.²² The solute radius was calculated to be 1.22 nm. The membrane used has a pore diameter reported by the manufacturer as 4.8 nm.²³ ω_r is the differential hydrodynamic drag, which is calculated from Equation S6 in the appendix. The solution of the mass balance ODE for reaction-only is shown in Equation 5. This equation was fit to the reaction-only experimental data to obtain the reaction rate used in the model.

$$D_{ij} = \frac{T}{\epsilon\beta\omega_r} k_p l \quad [\text{Eq. 4}]$$

$$C(t) = C_0 e^{-kt} \quad [\text{Eq. 5}]$$

The model inputs were k , D_{ij} , a distance mesh, and a time mesh. The distance mesh input for the model was a vector that was the same length as the experimental results that was equally spaced from 0 to L . Measurements were taken of the well of the flow dialysis chamber, which had a diameter of 0.9 cm and a length of 0.88 cm. The boundaries of the time mesh input for the model were informed by the length of time of the physical experiments after being converted into dimensionless time using Equation 2.3. The time mesh was an equally spaced vector from zero to the final dimensionless time value and was also the same length as the experimental results. The model outputs a three-dimensional visualization of the solution as well as a matrix of concentrations at each distance and time point.

To compare the spatial and temporal results from the PDE model with the solely temporal experimental results, the average predicted concentration of each time point computed by the analytical model was calculated. Each well in the physical experiments was assumed to be well mixed. First the solution matrix was multiplied by the experimental initial concentration to make it dimensional. Then, the area under the concentration v. distance profile for each point of the time mesh was computed to obtain a total mass. Finally, the total mass for each time point was then divided by L to obtain an average concentration of the well at each time point. The predicted average concentration of the well was

then plotted against the experimentally measured concentration.

End Matter

Author Contributions and Notes

G.H. and K.H. created the analytical PDE model, did experimental data analysis with ODE equations and analytical PDE model, and performed statistical analysis. B.H. advised the creation of the analytical PDE model and experimental data analysis. B.H. and W.G. advised the statistical analysis. W.A. and M.P. conducted *in vitro* experiments and obtained experimental data. W.A., G.H., K.H., and M.P. wrote the report. W.G. and B.H. read and provided edits for the report. The authors declare no conflict of interest.

Acknowledgments

This work was funded by the NIH grant R25 EB023841 via the UVA Biomedical Engineering Clinical Scholars program.

We also want to thank Timothy E. Allen Ph.D, Cooper Yurish, Sam Thapaliya, Eddy Trujillo, and Van Spinelli for their contributions.

Supplemental Figures

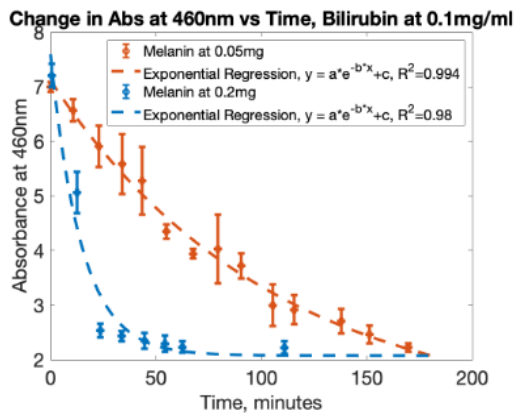


Figure S1: Photoconversion of high bilirubin solutions at high and low melanin concentrations.¹⁴

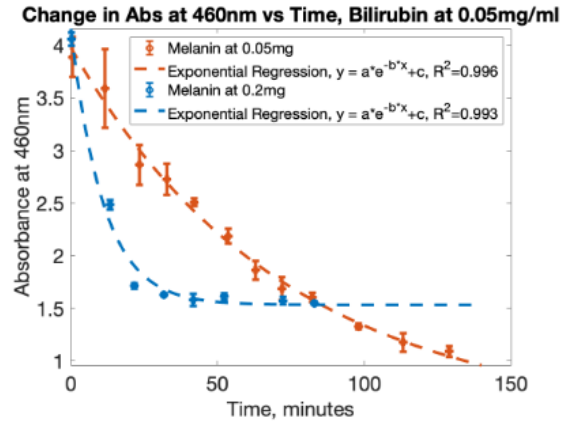


Figure S2: Photoconversion of low bilirubin solutions at high and low melanin concentrations.¹⁴

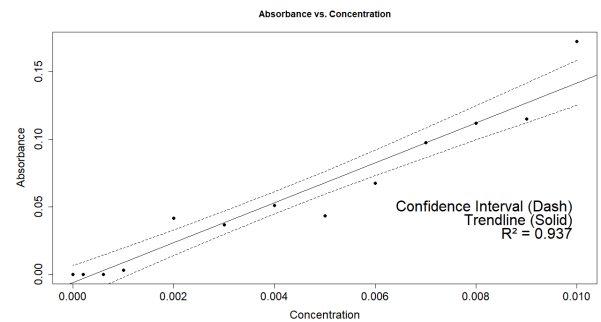


Figure S3: Bilirubin calibration curve with 95% confidence intervals

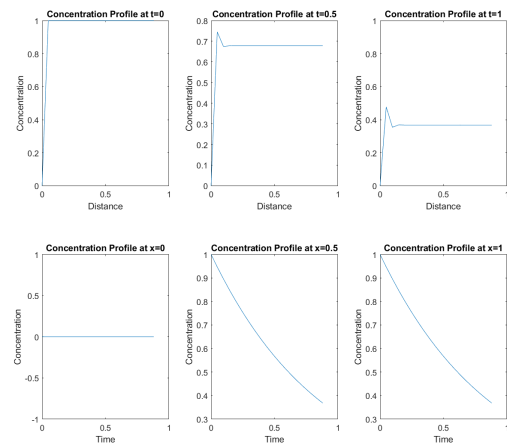


Figure S4: Spatial and temporal slices generated from the MATLAB pdepe solver show a decrease in concentration profile across both dimensions

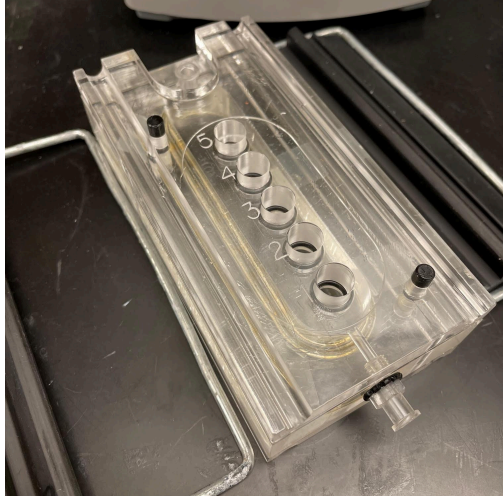


Figure S5: Image of the flow dialysis unit used for diffusion-only and diffusion-reaction experiments.

Supplemental Equations

$$A(t) = \alpha e^{-bt} + c \quad [\text{Eq. S1}]$$

$$\text{delta} = \text{Abs}_{t=0} - \text{Abs}_{t=\text{end}} \quad [\text{Eq. S2}]$$

$$\beta = (1 - \lambda)^2 \quad [\text{Eq. S3}]$$

$$\lambda = \frac{2a}{d} \quad [\text{Eq. S4}]$$

$$a = \frac{3MW}{4\pi\rho N_a} \quad [\text{Eq. S5}]$$

$$\omega_r = 1 - 2.1\lambda + 2.09\lambda^3 - 0.95\lambda^5 \quad [\text{Eq. S6}]$$

References

1. Shirzadfar, H., Amirzadeh, P., & Hajinorozi, M. H. (2019). A comprehensive study over the jaundice causes and effects on newborns and reviewing the treatment effects. *International Journal of Biosensors & Bioelectronics*, 5(4), 107–112. <https://doi.org/10.15406/ijbsbe.2019.05.00162>
2. Woodgate, P., & Jardine, L. A. (2011). Neonatal jaundice. *BMJ Clinical Evidence*, 2011, 0319.
3. Kemper, A. R., Newman, T. B., Slaughter, J. L., Maisels, M. J., Watchko, J. F., Downs, S. M., Grout, R. W., Bundy, D. G., Stark, A. R., Bogen, D. L., Holmes, A. V., Feldman-Winter, L. B., Bhutani, V. K., Brown, S. R., Maradiaga Panayotti, G. M., Okechukwu, K., Rappo, P. D., & Russell, T. L. (2022). Clinical Practice Guideline Revision: Management of Hyperbilirubinemia in the Newborn Infant 35 or More Weeks of Gestation. *Pediatrics*, 150(3), e2022058859. <https://doi.org/10.1542/peds.2022-058859>
4. Queensland Clinical Guidelines. (2022). *Neonatal Jaundice* (Guideline No. MN22.7-V9-R27). Retrieved from <http://www.health.qld.gov.au/qcg>
5. Ennever, J. F., McDonagh, A. F., & Speck, W. T. (1983). Phototherapy for neonatal jaundice: optimal wavelengths of light. *The Journal of pediatrics*, 103(2), 295–299. [https://doi.org/10.1016/s0022-3476\(83\)80370-9](https://doi.org/10.1016/s0022-3476(83)80370-9)
6. Onesimo, R., Fioretti, M., Pili, S., Monaco, S., Romagnoli, C., & Fundarò, C. (2011). Is heel prick as safe as we think?. *BMJ case reports*, 2011, bcr0820114677. <https://doi.org/10.1136/bcr.08.2011.4677>
7. Shah, V. S., & Ohlsson, A. (2011). Venepuncture versus heel lance for blood sampling in term neonates. *The Cochrane database of systematic reviews*, 2011(10), CD001452. <https://doi.org/10.1002/14651858.CD001452.pub4>
8. Onks, D., Silverman, L., & Robertson, A. (1993). Effect of melanin, oxyhemoglobin and bilirubin on transcutaneous bilirubinometry. *Acta paediatrica (Oslo, Norway : 1992)*, 82(1), 19–21. <https://doi.org/10.1111/j.1651-2227.1993.tb12507.x>
9. Sarici, S. U., Serdar, M. A., Korkmaz, A., Erdem, G., Oran, O., Tekinalp, G., Yurdakök, M., & Yigit, S. (2004). Incidence, course, and prediction of hyperbilirubinemia in near-term and term newborns. *Pediatrics*, 113(4), 775–780. <https://doi.org/10.1542/peds.113.4.775>
10. Varughese, P. M., Krishnan, L., & Ravichandran. (2018). Does color really matter? Reliability of transcutaneous bilirubinometry in different skin-colored

- babies. *Indian Journal of Paediatric Dermatology*, 19, 315–320.
11. Mahmoud, B. H., Hexsel, C. L., Hamzavi, I. H., & Lim, H. W. (2008). Effects of visible light on the skin. *Photochemistry and photobiology*, 84(2), 450–462. <https://doi.org/10.1111/j.1751-1097.2007.00286.x>
 12. Lamola, A. A., & Russo, M. (2014). Fluorescence excitation spectrum of bilirubin in blood: a model for the action spectrum for phototherapy of neonatal jaundice. *Photochemistry and photobiology*, 90(2), 294–296. <https://doi.org/10.1111/php.12167>
 13. Xiong, T., Tang, J., & Mu, D. Z. (2012). *Zhongguo dang dai er ke za zhi = Chinese journal of contemporary pediatrics*, 14(5), 396–400.
 14. Yurish, C., Thapaliya, S., Trujillo, E., Spinelli, V., & Guilford, W. (2023). *Design of a Skin-Tone Inclusive Technique for the Non-Invasive, Transcutaneous Measurement of Bilirubin*. <https://doi.org/10.18130/flbz-5985>
 15. Outlaw, F., Nixon, M., Odeyemi, O., MacDonald, L. W., Meek, J., & Leung, T. S. (2020). Smartphone screening for neonatal jaundice via ambient-subtracted sclera chromaticity. *PloS one*, 15(3), e0216970. <https://doi.org/10.1371/journal.pone.0216970>
 16. Uchida, Y., Takahashi, Y., Morimoto, Y., et al. (2022). Noninvasive monitoring of bilirubin photoisomer excretion during phototherapy. *Scientific Reports*, 12, 11798. <https://doi.org/10.1038/s41598-022-16180-9>
 17. Hahm, J. S., Ostrow, J. D., Mukerjee, P., & Celic, L. (1992). Ionization and self-association of unconjugated bilirubin, determined by rapid solvent partition from chloroform, with further studies of bilirubin solubility. *Journal of lipid research*, 33(8), 1123–1137.
 18. Tetko, I. V., Gasteiger, J., Todeschini, R., Mauri, A., Livingstone, D., Ertl, P., Palyulin, V. A., Radchenko, E. V., Zefirov, N. S., Makarenko, A. S., Tanchuk, V. Y., & Prokopenko, V. V. (2005). Virtual computational chemistry laboratory - design and description. *Journal of Computer-Aided Molecular Design*, 19(6), 453–463.
 19. Nii, K., Okada, H., Itoh, S., et al. (2021). Characteristics of bilirubin photochemical changes under green light-emitting diodes in humans compared with animal species. *Scientific Reports*, 11, 6391. <https://doi.org/10.1038/s41598-021-85632-5>
 20. Mathworks, Natick, MA
 21. Azhar, O., Jahan, Z., Sher, F., Niazi, M. B. K., Kakar, S. J., & Shahid, M. (2021). Cellulose acetate-polyvinyl alcohol blend hemodialysis membranes integrated with dialysis performance and high biocompatibility. *Materials Science & Engineering. C, Materials for Biological Applications*, 126, 112127. <https://doi.org/10.1016/j.msec.2021.112127>
 22. Fournier, R. L. (2011). *Basic Transport Phenomena in Biomedical Engineering, Third Edition*. CRC Press.
 23. *Fisher Science Education Seamless cellulose dialysis tubing - protein analysis reagents, dialysis and desalting*. (n.d.). https://www.fishersci.com/shop/products/seamless-cellulose-dialysis-tubing-16/S25645C?emb_id=pp_usorderconfirmation_producttitle